Calculation of a Current Vector Trajectory for Enhanced Operation of Synchronous Reluctance Generators Including Saturation

Hoffer Alvaro E., Moncada Roberto H., Pavez-Lazo Boris J., Tapia Juan A., Laurila Lasse

DOI: 10.1109/TIE.2022.3161820

Calculation of a Current-Vector Trajectory for Enhanced Operation of Synchronous Reluctance Generators Including Saturation

Alvaro E. Hoffer, Roberto H. Moncada, *Member*, *IEEE*, Boris J. Pavez-Lazo, Juan A. Tapia, *Senior Member*, *IEEE*, and Lasse Laurila

***Abstract*—This paper proposes a simple method to calculate a current-vector trajectory for enhanced operation of electric power generation system based on a synchronous reluctance machine (SynRM). Due to magnetic saturation and cross magnetization, the performance and torque capability of a SynRM vary according to the position and value of the stator current. State of the art control methods usually assume parameters with constant values, especially the inductance, neglecting saturation, leading to possible uncertainty in the machine operation. Therefore, a current-vector trajectory to operate this type of machine, as a generator, in an extended speed range, with enhanced performance and considering magnetic saturation is proposed. A straightforward algorithm based on the inductance characteristic of the machine is used to calculate the trajectory of the stator current vector. This trajectory is evaluated via numerical simulation of an experimentally validated finite element model of a SynRM. The results show that the proposed current-vector trajectory can improve the torque capability to 5 % concerning the estimated trajectory without considering saturation. Experimental results are also provided to demonstrate the enhanced operation of the generator.**

***Index Terms*—Electromagnetic analysis, energy efficiency, finite element analysis, generators, inductance, magnetic saturation, synchronous reluctance generator, torque, vector control.**

I. Introduction

SYNCHRONOUS reluctance machines (SynRMs) are a good alternative for use in renewable energy applications because of their several advantages such as high efficiency, compact size, robustness, and fault tolerance [1], [2]. Compared to permanent magnet synchronous machine (PMSM), the SynRM is free of magnets, therefore, this reduces manufacturing and maintenance costs [3], [4]. Researchers continuously propose new designs to boost the performance of a SynRM, as it is shown in [5]–[7].

Synchronous reluctance generators (SynRGs) have been studied for renewable energy applications, such as wind energy [1], [8]–[10]. Since they are machines that can operate in a wide range of speeds, it makes them suitable for variable speed wind power generation. However, to achieve an efficient energy conversion, it is essential that the machine operates with an appropriated control that takes advantage of its main capabilities. In [11], it was reported a control scheme for extensive speed range operation of a SynRM drive that complies with current and voltage rating constraints. The study results showed that the proposed control algorithm is capable of driving the machine in maximum torque per ampere, flux weakening, and maximum torque per volt while achieving minimum losses in every working condition. In [12], a control strategy for a SynRG that explores the operating limits of the generator in a wide range of speed was presented. It was proposed a path for the current reference vector based on the machine parameters which does not consider saturation.

Researchers have stated that the main performance of the SynRM is limited by its magnetic characteristic, especially the saturation phenomena which behaves differently in the direct axis and in the quadrature axis [13], [14]. In this last article, the authors said that saturation can be considered more easily if flux linkages are used as state variables rather than current. In [15], a method to maximize the operating efficiency in a SynRM that takes into consideration the magnetic saturation was proposed. In [16], it was reported that including the saturation by determining the trajectory for the current reference vector using finite element analysis (FEA) of the machine is computationally expensive and time-consuming. In [17] saturation is taken into account to propose a Maximum Torque per Ampere (MTPA) technique from a magnetic model of SynRM, which is parameterized from offline tests.

The present study is a continuation of the previous work reported in [16], where the finite element (FE) model of a commercial SynRM is presented and validated through simulation results only. The aim of this paper is to contribute to the development of a more efficient energy production by improving the performance of SynRG for electric power generation with a focus on renewable energy applications. In this way, this research proposes a simple method to calculate a current-vector trajectory, that considers the effects of saturation

This reasearch was supported by the Vicerrectoría de Investigación y Postgrado (VRIP) of the Universidad de La Frontera, Temuco, Chile, and the Agencia Nacional de Investigación y Desarrollo (ANID), Chile through Projects FONDECYT 11130709 and FONDECYT 1201667. *(Corresponding author: Alvaro E. Hoffer)*

Alvaro E. Hoffer, Roberto H. Moncada, and Boris J. Pavez-Lazo are with the Department of Electrical Engineering, Universidad de La Frontera, Temuco, 4811230, Chile (e-mail: alvaro.hoffer@ufrontera.cl; roberto.moncada@ufrontera.cl; boris.pavez@ufrontera.cl).

Juan A. Tapia is with the Department of Electrical Engineering, University of Concepción, Concepción, 4070386, Chile (e-mail: juan.tapia@udec.cl).

Lasse Laurila is with the Department of Electrical Engineering, LUT University, 53851 Lappeenranta, Finland (e-mail: lasse.laurila@lut.fi).

to operate the SynRG in a wide range of speed. It is intended to calculate the trajectory for the current reference vector by using the experimentally obtained inductance characteristic of the machine. This procedure presents advantages compared with FEA since no geometry and material information of the machine neither complex computing calculation are required. The machine performance when it operates under the trajectory calculated with the proposed method is demonstrated via numerical simulation (FEA) and experimental tests. The simplicity of the proposed algorithm makes it suitable to be implemented in microcontrollers commonly used for power converters.

II. The Synchronous Reluctance Generator

A three-phase SynRG can be described by a set of equations in the rotating d-q reference frame attached to the rotor [1]

$$u_{\mathrm{d}} = -R_{\mathrm{s}} i_{\mathrm{d}} + \frac{d\psi_{\mathrm{d}}}{dt} - \omega_{\mathrm{r}} \psi_{\mathrm{q}} \quad \psi_{\mathrm{d}} = -L_{\mathrm{d}} i_{\mathrm{d}}, \tag{1}$$

$$u_{\mathrm{q}} = -R_{\mathrm{s}} i_{\mathrm{q}} + \frac{d\psi_{\mathrm{q}}}{dt} + \omega_{\mathrm{r}} \psi_{\mathrm{d}} \quad \psi_{\mathrm{q}} = -L_{\mathrm{q}} i_{\mathrm{q}} \tag{2}$$

where u_{d}, u_{q} are d- and q-axes stator voltages, i_{d}, i_{q} are d- and q-axes stator currents, ψ_{d}, ψ_{q} are d- and q-axes components of the stator flux linkage, L_{d}, L_{q} are d- and q-axes inductances, ω_{r} is the electrical angular velocity, and R_{s} is the stator winding resistance per phase. From this model, the average electromagnetic torque can be obtained as

$$T_{\mathrm{em}} = \frac{3}{2} p \left(\psi_{\mathrm{d}} i_{\mathrm{q}} - \psi_{\mathrm{q}} i_{\mathrm{d}} \right) = -\frac{3}{2} p \left(L_{\mathrm{d}} - L_{\mathrm{q}} \right) i_{\mathrm{d}} i_{\mathrm{q}}, \tag{3}$$

where p is number of pole pairs of the machine and the factor 3/2 results from the transformation of the electrical stator quantities into the synchronous rotor frame. From (3), it is important to note that the torque production capability depends on the difference between the d- and q-axes inductances $(L_{\mathrm{d}} - L_{\mathrm{q}})$, which is known as saliency. A phasor diagram of a SynRM in the d-q frame with generator convention is shown in Fig. 1, where κ is the angle of the stator current vector I_{s} with respect to the rotor d-axis, ϕ is the phase angle between stator current and terminal voltage U_{s}, and δ is the angle of the stator flux-linkage vector Ψ_{s} in the rotor reference frame.

In general, it is common to assume constant values for L_{d} and L_{q}. However, due to magnetic saturation and cross-saturation effects, the magnetic circuit of the machine becomes nonlinear, and the inductances change. Fig. 2 shows the variation of the inductances as a function of the currents i_{d} and i_{q} in a commercial 11 kW synchronous reluctance motor calculated from FE model. Note that both inductances diminish their values as the current increases, yet, it becomes appreciable in the d-axis at a value of current higher than in the q-axis. This is because of the abundant amount of iron along the d-axis magnetic path compared with the q-axis, where, besides the flux barriers, only the iron bridges are present, which saturate quickly with low current. The effect of saturation in flux linkage and torque of the commercial machine as a generator for different constant current values is shown in Fig. 3. The dashed lines correspond to parameter curves for inductance with constant value at rated operation (i.e. without saturation), while the solid lines are obtained from

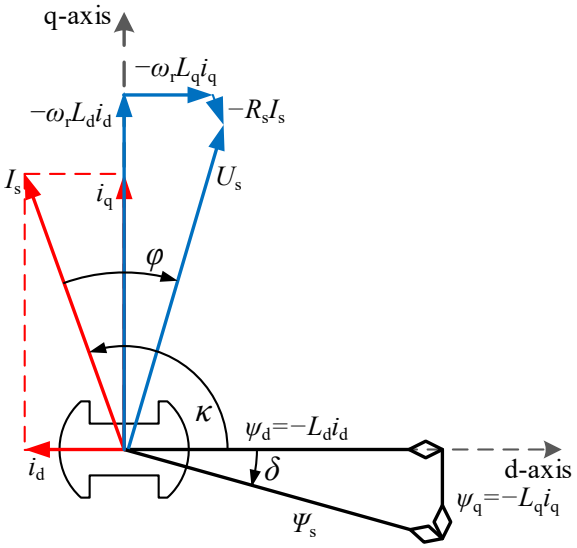

Fig. 1. Phasor diagram of a SynRM in generator mode.

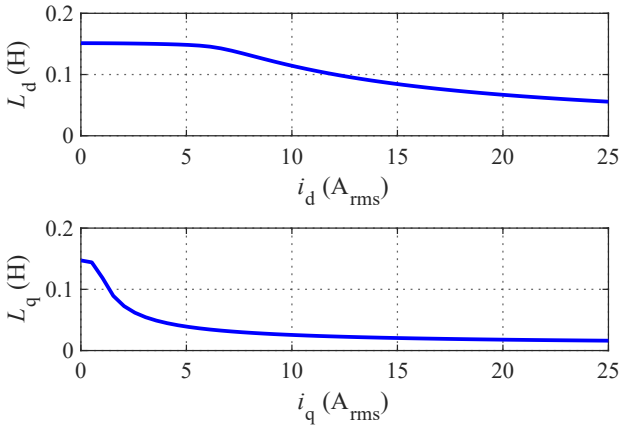

Fig. 2. Variation of inductances L_{d} and L_{q} in a SynRM as a function of current considering magnetic saturation.

FEA considering the saturation effects. The circles are the measured values. From these results, it is clear that there is a good agreement between FEA and experimental values, but not with constant-inductance (CI) model. Fig. 3(a) indicates that at different constant current values, the stator flux linkage becomes saturated (nonlinear relationship). Another consequence of saturation is the modification of the angle of the stator current vector when the machine develops the maximum torque. Note that, as the current increases, the current angle for maximum torque decreases, deflecting from the 135º predicted by (3). In addition, the torque values predicted by FEA and experimental tests are lower than the CI model.

III. High Efficiency Control Strategy

The conversion of energy from renewable sources such as wind energy should be efficient and capable of operating in a wide range of speeds to increase energy harvesting and availability. It is found in the literature that the SynRM operates efficiently with different operating modes according to the speed and load, such as: Maximum Torque per Ampere (MTPA) at

This article has been accepted for publication in IEEE Transactions on Industrial Electronics. This is the author's version which has not been fully edited and content may change prior to final publication. Citation information: DOI 10.1109/TIE.2022.3161820

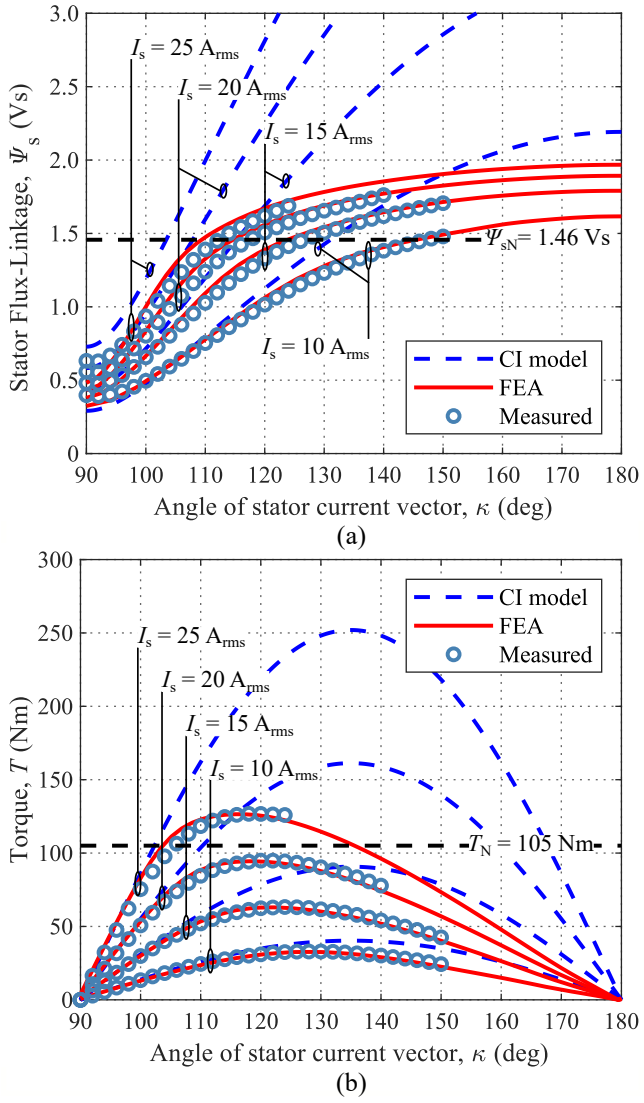

Fig. 3. Effect of saturation in (a) constant current stator flux-linkage curves and (b) constant torque curves.

low torque and low speed, Constant Flux (CF) from medium to rated torque and low speed, Flux Weakening (FW) at medium and high speed and Maximum Torque per Volt (MTPV) at high speed. With these operating modes, it is possible to take full advantage of the energy conversion capacity in each speed range, reducing losses, and hence achieving an efficient operation.

A control strategy to operate the SynRM in generator mode is presented in [12]. This strategy minimizes mainly the Joule losses. It complies with the constraints imposed by the safe operation of the machine (maximum values of flux linkage, voltage, and current) while maximizes the output power. The trajectory of the vector of current for this strategy is depicted in Fig. 4 (dashed line). However, it does not consider saturation, leading to low utilization of the machine capabilities.

The high-efficiency trajectory (HET) of the stator current vector considering the saturation is calculated in [16]. In this case, the authors use FEA to find the points for MTPA, CF, FW, and MTPV. This trajectory is also shown in Fig. 4 (solid line). Note that the machine is capable of developing more torque with the FEA-based HET compared with the CI-based HET. Even though this procedure produces good results, it is computationally expensive and time-consuming since it is necessary to build a FE model of the SynRM, which could be challenging, especially for commercial off-the-shelf units where usually all geometrical and construction data and material information are not available.

IV. Method for Calculation of the HET Considering Saturation

Neglecting cross-coupling, the performance of the SynRM, including saturation effects, can be estimated from its inductance characteristics. Then, the points that describe the HET can be found by computing the linear model of the SynRM with variable values of L_d and L_q. As can be seen in Fig. 2, both L_d and L_q curves present a soft variation, which means that the inductance characteristic can be easily reconstructed through linear interpolation with a low amount of $L\,(i)$ points.

In normal operation of SynRM (i.e., not exceeding maximum stator flux, voltage and current) the q-axis current could vary from zero to the rated value and the $L_q\,(i_q)$ characteristic would need to be known for the whole range of current. However, if the stator flux is kept within the rated value, the d-axis current will be, at most, one-third of the rated stator current (i.e., 0.3 pu) as seen in Fig. 2, then the $L_d\,(i_d)$ characteristic could be known only in the first third of the current range. Moreover, since the saturation along the d-axis is appreciable only at high current, very few points (i.e., at most three points) could be enough to describe the d-axis inductance curve.

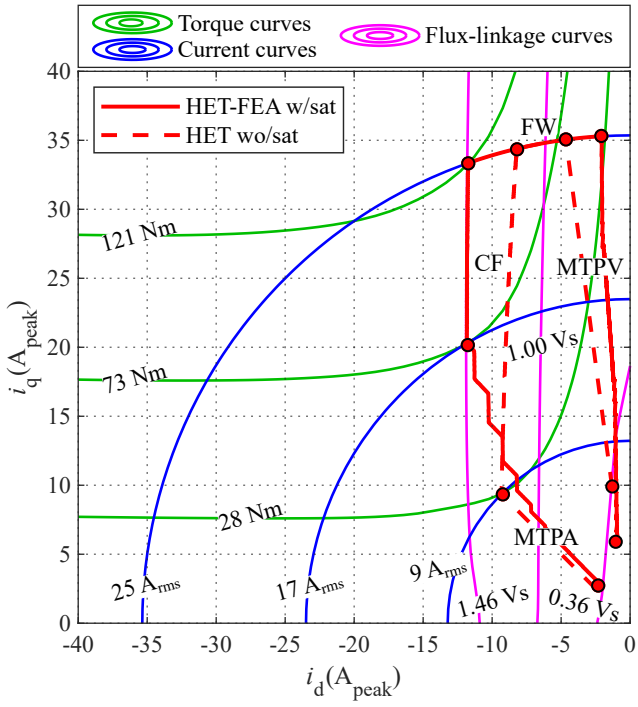

Fig. 4. Trajectories of stator current vector to produce the machine capability curves.

From the previous analysis, it can be stated that the HET points can be obtained by a simple algorithm based on a small look-up-table that contain information about the inductance characteristic of the machine.

A. Inductance Measurement

There are several methods to estimate or to measure the d-axis and q-axis inductances that can be applied to SynRM [18], [19]. It is not the aim of this paper to discuss or to propose a method for inductance estimation but rather to use this information to calculate the references for high-efficiency operation. The inductances L_d and L_q are estimated with the AC locked rotor test [20]. In this test, the rotor d-axis is aligned with the stator magneto motive force (MMF). Once aligned the rotor, it is locked mechanically to maintain this position. Then, single phase AC voltage U_AC at constant frequency f is applied to the stator winding according to Fig. 5(a) and the resulting AC current I_AC is measured.

The d-axis inductance is calculated as

$$L_\mathrm{d} = \frac{\sqrt{\left(U_\mathrm{AC}/I_\mathrm{AC}\right)^2 - R_\mathrm{s}^2}}{2\pi f}. \tag{4}$$

To calculate the q-axis inductance, the stator windings are reconnected according to Fig. 5(b) without unlocking the rotor. With this connection, the stator MMF is applied to the rotor q-axis. AC voltage is applied and the drawn current is measured. The q-axis inductance is calculated as

$$L_\mathrm{q} = \frac{\sqrt{\left(2U_\mathrm{AC}/I_\mathrm{AC}\right)^2 - R_\mathrm{s}^2}}{2\pi f}. \tag{5}$$

To obtain the inductance profile, different measurements are performed with several values of AC currents I_AC which are obtained by variation of the AC voltage U_AC but limited to the allowable values.

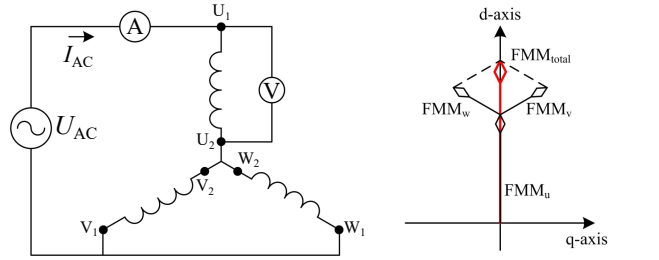

(a) Connection for d-axis

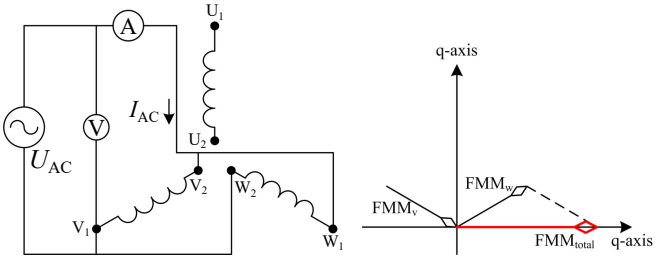

(b) Connection for q-axis

Fig. 5. Stator winding connection for AC locked rotor test.

B. HET Calculation

To find the i_d-i_q current combinations that compose the HET, the following relationship are used

$$\psi_\mathrm{d} = -L_\mathrm{d}\left(i_\mathrm{d}\right) i_\mathrm{d} \quad \psi_\mathrm{q} = -L_\mathrm{q}\left(i_\mathrm{q}\right) i_\mathrm{q} \tag{6}$$

$$i_\mathrm{d} = \sqrt{2} I_\mathrm{s} \cos\left(\kappa\right) \quad i_\mathrm{q} = \sqrt{2} I_\mathrm{s} \sin\left(\kappa\right), \tag{7}$$

where $L_\mathrm{d}\left(i_\mathrm{d}\right)$ and $L_\mathrm{q}\left(i_\mathrm{q}\right)$ are the look-up-tables that contain the points that describe the inductance characteristic of the machine, I_s is the RMS value of the stator current and κ is the angle of the stator current vector from the d-axis. Then, the torque considering the saturation effects can be expressed as

$$T = -\frac{3}{2} p \left(L_\mathrm{d}\left(i_\mathrm{d}\right) - L_\mathrm{q}\left(i_\mathrm{q}\right)\right) I_\mathrm{s}^2 \sin\left(2\kappa\right), \tag{8}$$

and the total stator flux and current

$$\Psi_\mathrm{s}{}^2 = \psi_\mathrm{d}{}^2 + \psi_\mathrm{q}{}^2 \leq \left(\sqrt{\frac{2}{3}} \frac{1}{p} \frac{U_\mathrm{s,\,max}}{\Omega_\mathrm{r}}\right)^2 = \left(\Psi_\mathrm{s,\,max}\right)^2 \tag{9}$$

$$i_\mathrm{d}^2 + i_\mathrm{q}^2 = 2I_\mathrm{s}^2 \leq 2I_\mathrm{sN}^2, \tag{10}$$

where Ψ_s and $\Psi_\mathrm{s,max}$ are the total and maximum stator flux-linkage respectively, $U_\mathrm{s,max}$ is the RMS value of the maximum fundamental line-to-line stator voltage, and Ω_r is the mechanical rotational speed.

Fig. 6 shows a flowchart of the procedure to compute the proposed trajectory. The algorithm consists as follows:

1) Calculate from (8) the curve of torque as a function of the angle of current κ for different values of stator current I_s. Then, find the maximum value of torque (T_MTPA) and the angle of current that produce it (κ_MTPA) for each value of stator current $(I_\mathrm{s,MTPA})$. These points correspond to the maximum-torque-per-ampere section.
2) Evaluate the feasibility of the MTPA points computing from (9) the total stator flux linkage. If the flux linkage exceeds $\Psi_\mathrm{s,\,max}$, then solve (6), (7) and (9) to find the angle of current (κ_CF) that produces the rated stator flux linkage Ψ_sN for the given stator current $(I_\mathrm{s,CF})$ and calculate the new torque (T_CF) from (8). These points correspond to the constant-flux segment.
3) For operating speeds greater than the rated speed, calculate torque as a function of flux linkage by solving (3), (6) and (9) to find the $(\psi_\mathrm{d}, \psi_\mathrm{q})$ combination that produces the maximum torque for a given mechanical speed. Then, from these flux linkage values, find the corresponding $(i_\mathrm{d}, i_\mathrm{q})$ combination that produces these flux linkages. If the found combination of current satisfies (10), then calculate the angle of current (κ_MTPV) and save the value of the stator current $(I_\mathrm{s,MTPV})$ and torque (T_MTPV). The points calculated with this procedure correspond to the maximum-torque-per-volt section.
4) If the $(i_\mathrm{d}, i_\mathrm{q})$ combination found previously does not satisfy (10), then solve (9) and (7) to find the angle of current (κ_FW) that force the fulfillment of (9) for the given speed considering rated stator current. These points correspond to the FW operation.

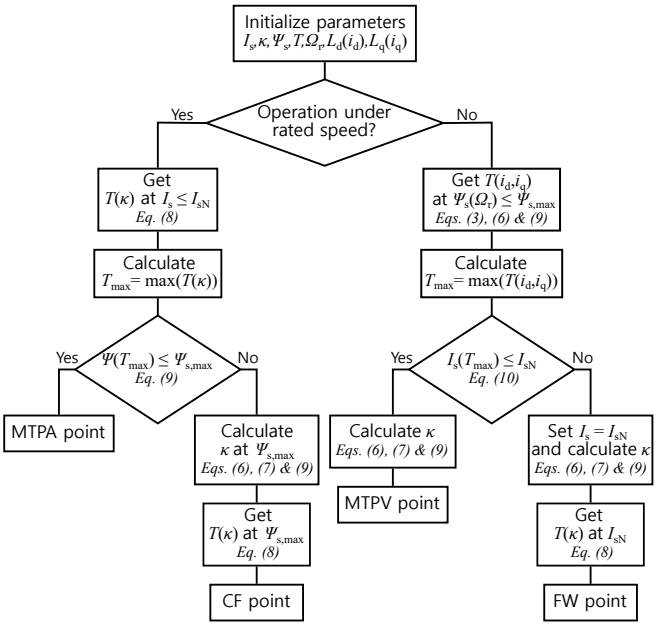

Fig. 6. Flowchart to calculate the HET considering the effect of saturation

.

V. Evaluation and Experimental Validation of the Proposed Method

The method described in the previous section is employed to calculate the trajectory of the stator current vector that produces enhanced operation in an actual commercial off-the-shelf 11 kW SynRM. Table I shows main nameplate and geometrical parameters of the commercial machine. The inductance characteristic of the machine obtained from FEA (solid line) and experimental test (circle marks) is presented in Fig. 7. A close agreement between simulated and measured results is observed. However, it can also be observed that there is a disagreement in the q-axis inductance low current zone. Despite this, it does not affect the calculation of the proposed trajectory, since the FE model of the machine is used only to evaluate the machine performance.

A. Experimental Test Bench Setup and Control Scheme Outlook

The SynRM FEA model and proposed method were validated via experimental tests carried out in the test bench shown in Fig. 8. The SynRM under test is coupled to a 22 kW, 980 r/min, induction motor (IM) that operates as a prime mover (dynamometer motor). The input speed of the system is set by the dynamometer drive (ABB ACS 800-11), and the SynRM drive (DANFOSS FC 302) is configured to perform a field-oriented control (FOC) to the SynRM. FOC is implemented on a dSPACE 1103 platform which provides control over the SynRM converter. The scheme of connection of the experimental setup is shown in Fig. 9. Note that the SynRM drive is connected to the DC-link of the dynamometer drive, and this later is connected to the grid. For this connection scheme, the power flow goes from the SynRM to the DC-bus and then to the dynamometer. When the system is running, the grid only supplies the system losses to keep it operating.

The measurement of torque is performed with a torqueme-

TABLE I
Parameters and Ratings of the Commercial SynRM.

Parameter	Value
Rated power P_N (kW)	11
Rated mechanical speed n_N (rpm)	1000
Rated torque T_N (Nm)	105
Rated stator voltage U_{sN} (Vrms)	370
Rated stator current I_{sN} (Arms)	25
Rated frequency f_N (Hz)	33
Stator winding resistance per phase R_s (Ω)	0.3
d-axis inductance L_d @ rated operation (H)	0.150
q-axis inductance L_q @ rated operation (H)	0.021
Number of poles $2p$	4
Number of stator slots Q_s	36
Stator outer diameter D_{so} (mm)	260.0
Stator inner diameter D_{si} (mm)	166.0
Rotor outer diameter D_{ro} (mm)	165.0
Rotor inner diameter D_{ri} (mm)	53.5
Axial length l' (mm)	261.0
Winding connection	star

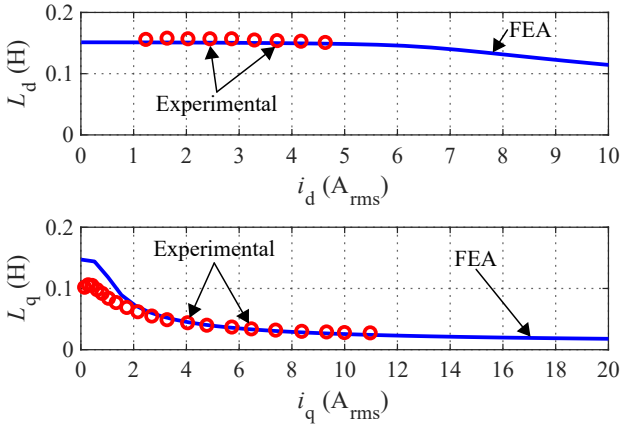

Fig. 7. Inductance characteristic of the commercial SynRM obtained by FEA and experimental tests.

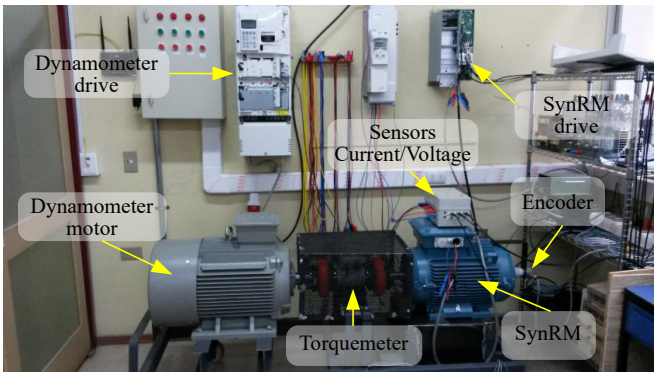

Fig. 8. Experimental test bench setup.

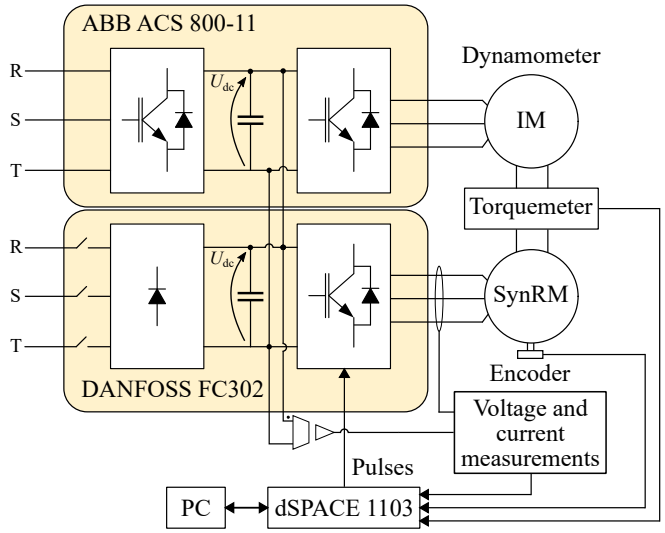

Fig. 9. Schematic view of the test setup. The DC voltage U_{DC} is common to both converters.

ter (Himmelstein MC48703V(2-3)CFZ) coupled to the shaft , where its output signal provides the magnitude and polarity of the mechanical torque. The rotor position is measured with an incremental encoder (SICK DFS60). The acquisition and processing of the data is executed in the dSPACE 1103 platform.

The current-control of the SynRM is achieved with adaptive proportional-integral (PI) controllers as presented in Fig. 10. The controller coefficients are calculated considering the non-linear relationships $L_{\mathrm{d}}\,(i_{\mathrm{d}})$ and $L_{\mathrm{q}}\,(i_{\mathrm{q}})$ obtained by experimental tests as shown in Fig. 7. The current references to follow the HET-prop. are given via look-up tables, that contain the values calculated with the proposed method.

B. Calculated HET

The experimental measurement of L_{d} and L_{q} are used to build the look-up-tables required to calculate the HET for the commercial SynRM. The look-up-tables contain only nine points for L_{d} and twenty points for L_{q}. The testing current spans from 1 Arms to 5 Arms (0.04 pu to 0.2 pu) for the d-axis and from 0.25 Arms to 12.5 Arms (0.01 pu to 0.5 pu) for the q-axis. The different HETs were evaluated by numerical simulation of a FE model of the actual commercial SynRM while HET calculated with the proposed method was evaluated experimentally.

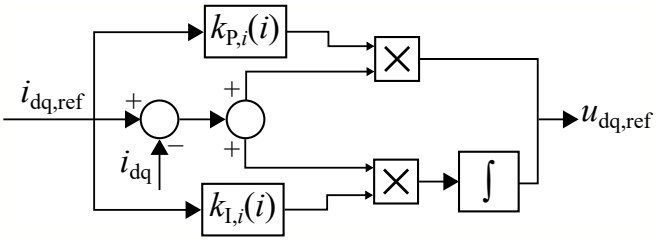

Fig. 10. Adaptive PI controller implemented in the SynRG under test.

Fig. 11 shows the polar diagram of the commercial SynRM, where the HET calculated with the proposed method (HET-prop. w/sat - dotted line) is compared with the trajectory obtained with the estimated trajectory without considering saturation (HET wo/sat - dashed line). Note that the trajectory obtained with the proposed method is very close to the HET obtained with FEA in the MTPA section, but it was obtained faster and requiring less computational cost than FEA. Furthermore, since there is some uncertainty in obtaining the inductances for the CI model, the HET-prop. is a feasible and safe option for generator operation.

The experimental test consisted in applying the current references to the machine running at a constant speed to measure current, voltage, power, and torque. The test was repeated for several speeds obtaining similar results. Finally, the experimental points shown in Figs. 12 are those obtained at rated speed 600rpm.

Figs. 12(a) and 12(b) show the torque and the flux linkage developed by the SynRM respectively when it operates under the HETs calculated by the different methods, while the circles are the measured values when the generator operates under the HET-prop. (MTPA and CF zone). Note that the HET-prop. leads the generator to develop the maximum torque until the stator current reaches 11 Arms without exceeding the stator flux-linkage limit, then, the machine operates with 80∼90% of Ψ_{sN}, but still increasing the developed torque until the stator current reaches I_{sN}. This current value is kept constant in the FW zone and it is diminished in the MTPV operation. The figures also show that the HET-prop. allows the machine to produce peak torque close to rated torque while maintaining I_{sN} and under $\Psi_{\mathrm{s,max}}$. The proposed trajectory can improve

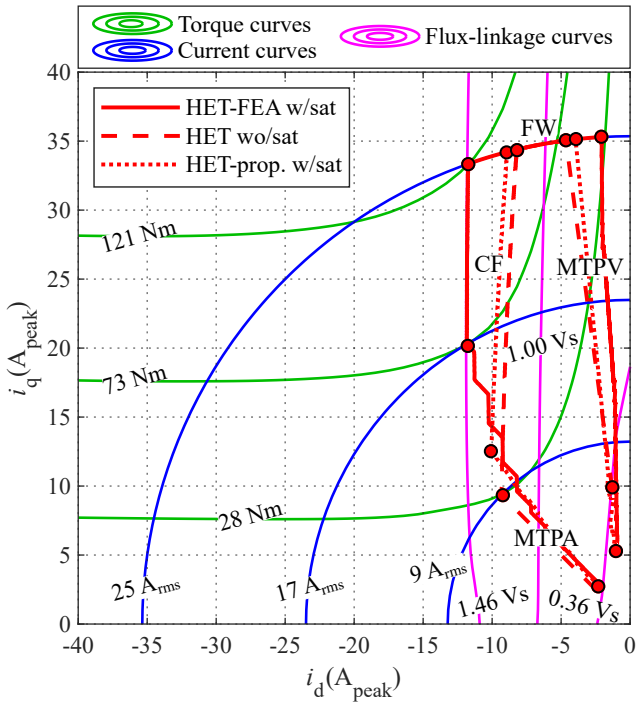

Fig. 11. HET obtained with the proposed method plotted in the polar diagram of the commercial SynRM.

the torque capability to 5% concerning the trajectory without considering saturation. The experimental results show a close agreement with the numerical simulation.

The generator efficiency under the different HETs are presented in Fig. 12(c). It is important to note that the theoretical efficiency of the machine operating under the HET-prop. shows differences with the measurements. It can be explained because no mechanical and additional losses were considered in the numerical simulations.

VI. Conclusion

A straight forward method for easy calculation of a trajectory for the stator current vector for enhanced operation of a SynRM was proposed in this paper.

Numerical simulation of an experimentally validated finite element model of an actual commercial off-the-shelf SynRM was performed to evaluate the trajectory. The results show that the proposed trajectory allows a better performance of the machine than the obtained trajectory that does not consider saturation.

The simplicity and low data and computing requirement of the proposed HET calculation method makes it possible to implement it in a regular microcontroller to serve as add-on in new power converters to be used to control SynRM.

References

[1] R. H. Moncada, H. A. Young, B. J. Pavez-Lazo, and J. A. Tapia, "A Commercial-Off-The-Shelf Synchronous Reluctance Motor as a Generator for Wind Power Applications," in *2015 IEEE International Electric Machines Drives Conference (IEMDC)*, DOI 10.1109/IEMDC.2015.7409029, pp. 6–12, 2015.

[2] D.-K. Ngo and M.-F. Hsieh, "Performance Analysis of Synchronous Reluctance Motor with Limited Amount of Permanent Magnet," *Energies*, vol. 12, DOI 10.3390/en12183504, no. 18, 2019.

[3] G. Almandoz, I. Gómez, G. Ugalde, J. Poza, and A. J. Escalada, "Study of Demagnetization Risk in PM Machines," *IEEE Transactions on Industry Applications*, vol. 55, DOI 10.1109/TIA.2019.2904459, no. 4, pp. 3490–3500, 2019.

[4] S. Stipetic, D. Zarko, and N. Cavar, "Adjustment of Rated Current and Power Factor in a Synchronous Reluctance Motor Optimally Designed for Maximum Saliency Ratio," *IEEE Transactions on Industry Applications*, vol. 56, DOI 10.1109/TIA.2020.2971442, no. 3, pp. 2481–2490, 2020.

[5] K. Wang, Z. Zhu, G. Ombach, M. Koch, S. Zhang, and J. Xu, "Torque ripple reduction of synchronous reluctance machines: Using asymmetric flux-barrier," *COMPEL - The international journal for computation and mathematics in electrical and electronic engineering*, vol. 34, DOI 10.1108/COMPEL-11-2013-0367, pp. 18–31, Jan. 2015.

[6] G. Boztas, O. Aydogmus, M. Caner, and H. Guldemir, "Design, optimisation and implementation of low-voltage synchronous reluctance motor for solar-powered systems," *IET Power Electronics*, vol. 12, DOI 10.1049/iet-pel.2018.5895, no. 7, pp. 1679–1685, 2019.

[7] Y. Bao, M. Degano, S. Wang, L. Chuan, H. Zhang, Z. Xu, and C. Gerada, "A Novel Concept of Ribless Synchronous Reluctance Motor for Enhanced Torque Capability," *IEEE Transactions on Industrial Electronics*, vol. 67, DOI 10.1109/TIE.2019.2914616, no. 4, pp. 2553–2563, 2020.

[8] P. Roshanfekr, S. Lundmark, B. Anvari, and T. Thiringer, "Investigation of Pole Number Selection in a Synchronous Reluctance Generator for Wind Applications," in *2017 IEEE International Electric Machines and Drives Conference (IEMDC)*, DOI 10.1109/IEMDC.2017.8002336, pp. 1–6, 2017.

[9] M. Alnajjar and D. Gerling, "Medium-Speed Synchronous Reluctance Generator as Efficient, Reliabile and Low-Cost Solution for Power Generation in Modern Wind Turbines," in *2018 International Symposium on Power Electronics, Electrical Drives, Automation and Motion (SPEEDAM)*, DOI 10.1109/SPEEDAM.2018.8445237, pp. 1233–1238, 2018.

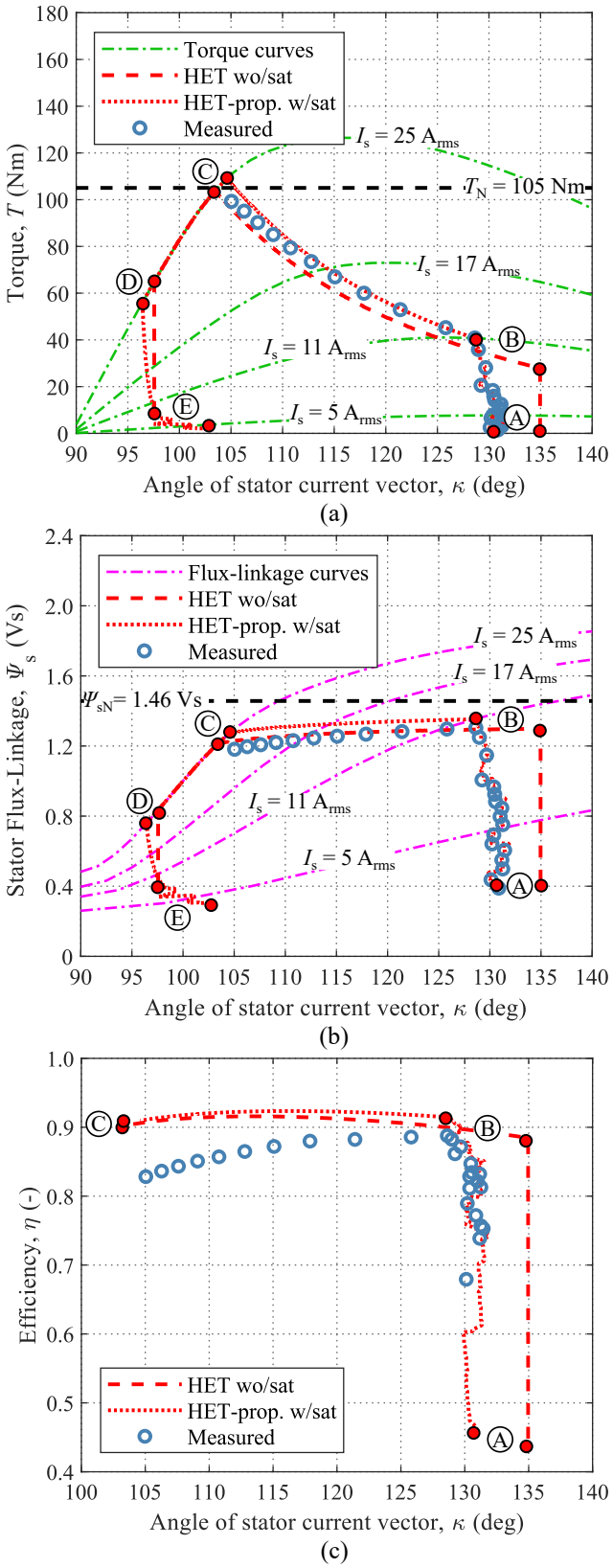

Fig. 12. (a) Torque, (b) stator flux-linkage, and (c) efficiency of the generator when it operates under the calculated HETs. The operating modes of the trajectories are defined as: A → B = MTPA; B → C = CF; C → D = FW; E → F = MTPV.

[10] Y. Wang and N. Bianchi, "Modeling and Investigation of Self-Excited Reluctance Generators for Wind Applications," *IEEE Transactions on Industry Applications*, vol. 55, DOI 10.1109/TIA.2019.2935931, no. 6, pp. 5809–5817, 2019.
[11] V. Manzolini, D. Da Rù, and S. Bolognani, "An Effective Flux Weakening Control of a SyRM Drive Including MTPV Operation," *IEEE Transactions on Industry Applications*, vol. 55, DOI 10.1109/TIA.2018.2886328, no. 3, pp. 2700–2709, 2019.
[12] R. H. Moncada, B. J. Pavez, J. A. Tapia, and J. Pyrhönen, "Operation Analysis of Synchronous Reluctance Machine in Electric Power Generation," in *2014 International Conference on Electrical Machines (ICEM)*, DOI 10.1109/ICELMACH.2014.6960575, pp. 2734–2739, 2014.
[13] A. Vagati, M. Pastorelli, F. Scapino, and G. Franceschini, "Impact of cross saturation in synchronous reluctance motors of the transverse-laminated type," *IEEE Transactions on Industry Applications*, vol. 36, DOI 10.1109/28.855958, no. 4, pp. 1039–1046, 2000.
[14] H. A. A. Awan, S. E. Saarakkala, and M. Hinkkanen, "Flux-linkage-based current control of saturated synchronous motors," *IEEE Transactions on Industry Applications*, vol. 55, DOI 10.1109/TIA.2019.2919258, no. 5, pp. 4762–4769, 2019.
[15] S. Yamamoto, H. Hirahara, J. B. Adawey, T. Ara, and K. Matsuse, "Maximum Efficiency Drives of Synchronous Reluctance Motors by a Novel Loss Minimization Controller With Inductance Estimator," *IEEE Transactions on Industry Applications*, vol. 49, DOI 10.1109/TIA.2013.2265071, no. 6, pp. 2543–2551, 2013.
[16] A. E. Hoffer, R. H. Moncada, B. J. Pavez, J. A. Tapia, and L. Laurila, "A High Efficiency Control Strategy for Synchronous Reluctance Generator Including Saturation," in *2016 XXII International Conference on Electrical Machines (ICEM)*, DOI 10.1109/ICELMACH.2016.7732503, pp. 39–45, 2016.
[17] A. Accetta, M. Cirrincione, M. C. D. Piazza, G. L. Tona, M. Luna, and M. Pucci, "Analytical formulation of a maximum torque per ampere (mtpa) technique for synrms considering the magnetic saturation," *IEEE Transactions on Industry Applications*, vol. 56, DOI 10.1109/TIA.2020.2993525, no. 4, pp. 3846–3854, 2020.
[18] T. Miller, J. Walker, and C. Cossar, "Measurement and Application of Flux-Linkage and Inductance in a Permanent-Magnet Synchronous Machine," in *Second International Conference on Power Electronics, Machines and Drives (PEMD 2004).*, vol. 2, DOI 10.1049/cp:20040369, pp. 674–678 Vol.2, 2004.
[19] M. Morandin and S. Bolognani, "Locked Rotor Characterization Tests of IPM/REL Synchronous Machine for Sensorless Drives," in *8th IET International Conference on Power Electronics, Machines and Drives (PEMD 2016)*, DOI 10.1049/cp.2016.0352, pp. 1–6, 2016.
[20] D. A. Gonzalez-Lopez, J. A. Tapia, R. Wallace, and A. Valenzuela, "Design and Test of an Axial Flux Permanent-Magnet Machine With Field Control Capability," *IEEE Transactions on Magnetics*, vol. 44, DOI 10.1109/TMAG.2008.2000543, no. 9, pp. 2168–2173, 2008.

Alvaro E. Hoffer was born in Temuco, Chile, in 1991. He received the B. Eng. and M. Eng. degrees in Electrical Engineering from the Universidad de la Frontera, Temuco, Chile, in 2016, and the double D.Sc. degree from the University of Concepción, Concepción, Chile, in cotutelle with the Lappeenranta-Lahti University of Technology LUT, Lappeenranta, Finland, in 2021. His current research interests include the field of electrical machines and drives, and renewable energies.

Roberto H. Moncada (S'05, M11) was born in Chillán, Chile. He received the Electrical Engineering Degree and the Doctor Degree in Electrical Engineering from the University of Concepción, Concepción, Chile in 2006 and 2012 respectively. Currently he is with the Universidad de La Frontera, Temuco, Chile as an Assistant Professor in the area of Electrical Machines. His research interest includes permanent-magnet machines design and control, synchronous reluctance machines, power electronics, renewable energy and energy efficiency.

Boris. J. Pavez-Lazo was born in Lota, Chile. He received the Electrical Engineering Diploma, the Magister Degree and the Doctor Degree in Electrical Engineering from the University of Concepción, Concepción, Chile in 1999, 2002 and 2010 respectively. Currently he is with the Universidad de La Frontera, Temuco, Chile as an Assistant Professor in the area of Power System. His research interest includes Power System and Non-Conventional Renewable Energy.

Juan A. Tapia (M'01, SM'18) received the B.Sc. and M.Sc. degrees in electrical engineering from the University of Concepción, Concepción, Chile, in 1991 and 1997, respectively, and the Ph.D. degree from the University of Wisconsin, WI, Madison, in 2002. From 2010 to 2014, he was a FiDiPro Fellow with the Academy of Finland, Lappeenranta University of Technology, Lappeenranta, Finland, where he conducts research on PM machine on LUT-Energia Group. Currently, he is working as an Associate Professor with the Department of Electrical Engineering, University of Concepción. His research interests include electrical machines design, numerical method for electromagnetic fields, and renewable energy.

Lasse Laurila was born in Helsinki, Finland, in 1971. He received the M.Sc., Lic. Tech., and D. Sc. degrees from the Lappeenranta University of Technology, Lappeenranta, Finland, in 1996, 2000, and 2004, respectively. His research interests include power electronic converters, variable-speed drives and their control. He is currently interested in energy efficient mobile electric drives. He is currently an Associate Professor at the Laboratory of Electrical Drives Technology, Lappeenranta University of Technology.